OpenMC Interpretation of FNS SINBAD Shielding Benchmark Experiments

Bamidele Ebiwonjumi*, Stefano Segantin, Ethan Peterson

Plasma Science and Fusion Center, Massachusetts Institute of Technology, 167 Albany Street, Cambridge, Massachusetts, United States
*Email: bamidele@mit.edu

Abstract

Fusion Neutron Source (FNS) clean benchmark experiments on tungsten, vanadium and beryllium assemblies from the Shielding Integral Benchmark Archive and Database (SINBAD) are analyzed to experimentally validate OpenMC (version 0.14.1-dev) fusion neutronics capabilities. The assemblies were irradiated with a 14 MeV D-T neutron source. Neutron spectra, photon spectra, reaction rates, gamma heating rates (GHR), and tritium production rates (TPR) are compared to measured data in the experimental assemblies and MCNP-6.2 results. In the tungsten case, slight overestimations of the experimental data are observed in the neutron spectra and the photon spectra agree well with the experiments. Most of the GHR agree with the measured data within the range of experimental uncertainty in the tungsten and vanadium assemblies. In the vanadium assembly, the calculated neutron spectra underestimate the experiments in the low energy region while the photon spectra are well calculated when compared to experiments. The most noticeable discrepancies with experimental data in the gamma heating are observed at detector positions closest to the source. For the reaction rates, notable discrepancies with experimental data are seen at the front and rear of the assemblies. Compared to experiments, the OpenMC neutron spectra are well predicted in the beryllium assembly, whereas the calculated fission reaction rate and TPR overestimates the experiments, an observation similar to that which has been reported by other authors. The average, overall *C*/*E* over 9 TPR and 7 GHR measurements are 1.03 ± 0.20 and 0.95 ± 0.14, respectively. In the case of verification, OpenMC results of the benchmark calculations indicate comparable accuracy to MCNP-6.2. In general, the validation exercise shows that OpenMC can be used to analyze the fusion neutronics shielding benchmark problems.

Keywords: OpenMC, Fusion Neutronics, FNS Clean Benchmarks, Verification and Validation.

I. Introduction

As activities ramp up towards adopting the open-source code OpenMC as one of the tools for fusion reactor design and neutronic analysis, it becomes important to benchmark its fusion neutronics capabilities. Although OpenMC has been used in the fusion community and benchmarked against other Monte Carlo (MC) codes for fusion neutronic parameters such as shutdown dose rate, tritium breeding, particle spectra, and nuclear heating, the benchmarking has been limited to a few experimental and computational benchmark cases [1,2,3,4]. Beyond these, it is important to extend the benchmark cases employed in OpenMC validation exercises, in particular making them publicly available and automated whenever possible. This would reduce the time required to rerun comparison for new releases of the code and reduce effort of the scientific community by avoiding duplication of effort. In addition, validation works on radiation shielding, deep penetration and variance reduction (VR) capabilities of OpenMC are sparse [5,6] and more is yet to be performed, especially as new features are added rapidly and the application programming interface (API) matures. OpenMC [7] is a community developed particle transport code whose development started at the Massachusetts Institute of Technology (MIT) in the USA and now at Argonne National Laboratory and by contributors from the reactor physics and fusion neutronics communities around the world.

As previously mentioned, few benchmark experiment analysis with Deuterium-Tritium (D-T) neutron sources have been published with OpenMC. This paper provides additional validation elements of OpenMC in interpreting fusion shielding experiments. This report is focused on the Fusion Neutron Source (FNS) clean benchmark experiments in the Shielding Integral Benchmark Archive and Database (SINBAD) [8]. SINBAD is jointly managed by the Radiation Safety and Information Computational Center (RSICC) and the Organization of Economic Cooperation Development (OECD) Nuclear Energy Agency (NEA) Data Bank and compiles evaluations of shielding benchmark experiments for computer code and nuclear data validation [9].

Verification and validation (V&V) of nuclear analysis tools are important to evaluate their bias, accuracy, and increase reliability in predicting the nuclear responses of interest. This is particularly important for fusion reactor design where geometries are complex, evolve rapidly, and have many downstream systems affected by neutrons. Development of OpenMC fusion neutronics capabilities is being carried out to tackle these challenges. The plan of this paper is as follows. First, a brief overview of OpenMC is given, highlighting its features. Second, the fusion

neutronics shielding benchmark experiments analyzed herein are presented alongside details of the experimental room, D-T target facilities, source information, details of neutron/photon detectors and experimental assemblies. These experiments are selected for the V&V of OpenMC calculation of radiation spectra, dosimetry reaction rates, gamma heating and tritium production rates. Third, we present the computational models, methods, and nuclear data libraries used to analyze the benchmark experiments. Fourth, for three FNS benchmarks, the fusion neutronics parameters calculated by OpenMC are compared to measured data and MCNP-6.2 results, and the agreements and discrepancies observed are discussed and analyzed. Fifth, the conclusions and perspectives are outlined.

II. OpenMC Monte Carlo Code

OpenMC is a three-dimensional, continuous-energy, neutron-photon transport MC code with capabilities for eigenvalue, burnup [10], fixed source, and neutron-photon coupled simulations. It was originally developed and validated for fission reactor physics design and analysis and is actively being developed by implementing several fusion neutronics, shielding and VR capabilities [1,2,3,4,5,6]. The code is written in C++ and allows for the creation of APIs. The code has a Python API that can be used to create model problem input files in the traditional Constructive Solid Geometry (CSG) and extensible markup language (XML) formats and postprocess simulation results. The open-source code is publicly available on the GitHub repository [11]. OpenMC uses HDF5 based data format for storing cross sections, angle-energy distributions and other data required during simulations. The HDF5 files can be generated from the ACE and/or ENDF files, or the user can employ pre-generated HDF5 data. The code can be run in parallel using the shared-memory parallelism via the OpenMP API and the message passing interface (MPI), with scalability to over 100,000 processors on modern supercomputers [7].

III. Fusion Neutronics Benchmark Experiments

Three benchmark cases are selected from SINBAD fusion neutronics shielding problems for the purposes of validating fixed source neutron and photon transport and prompt nuclear responses (tallies) with the application of weight windows (WW) for VR. We focus on experiments with source neutrons produced from D-T interactions. These benchmark experiments are from the Fusion Neutronics Source (FNS) facility at the Japanese Atomic

Energy Research Institute (JAERI), now Japan Atomic Energy Agency and are part of the SINBAD benchmark suite for shielding. Brief descriptions of the experiments considered in this paper are presented below. However, detailed descriptions of the benchmarks can be found in [12] and in the references contained in the following sections for each benchmark. Although the original purpose of the benchmarks was to validate nuclear data used in predicting nuclear responses in fusion reactors, the benchmark experiments are used here to validate the application of OpenMC to fusion specific use-cases. The benchmarks considered in this paper consist of tungsten and beryllium materials in quasi-cylindrical assemblies, and vanadium material in a cubical assembly. Benchmark experiments have been conducted in years past for materials of relevance in fusion reactors such as for tritium breeding, neutron multiplication, structural materials, plasma facing components, superconducting magnets and for shielding purposes.

The experiments were carried out at the JAERI FNS facility in Japan where 14 MeV D-T neutrons were produced by 350 keV deuteron beam coming from an accelerator, interacting with a tritium-titanium target containing 3.7×10^{11} Bq tritium. The beam current was 20 nA – 2 mA. The neutron yield on average was about 2×10^{11} n/s measured using the associated alpha particle method [12]. The target room has a 15 m × 15 m floor area, 9.1 m height, 1.15 m thick roof concrete, and 2 m thick vertical wall. To reduce neutron scattering from the floor, the target room floor is made of an iron grating. The tritium target is 1.8 m height above the floor, 2.75 m away from the west wall and 5.5 m from the south wall. A 0.9 m × 0.9 m port is present in the roof which is closed with a plug of concrete. The experimental assemblies were at least 4 m away from the room walls and floor, to minimize background neutrons and gammas from the walls and floor contributing to the measured data. Moreover, the experimental assemblies serve as shielding materials against the background neutrons. The distance between the target and experimental assemblies is 200 mm. The quasi-cylindrical assemblies (which are the assemblies made of tungsten and beryllium materials) are fastened inside frames of aluminum and mounted on a steel deck. The neutron flux spectrum is measured by three detectors covering three different energy ranges. A 14 mm diameter spherical NE213 liquid organic scintillation counter, a pair of proton recoil gas proportional counter (PRC), and the slowing down time method (SDT) was used to measure neutron spectrum above 2 MeV, between 20 keV to 1 MeV, and from 1 eV to 300 eV, respectively. A 40 mm diameter spherical BC537 liquid organic scintillation counter was used to measure the photon flux spectrum. The foil activation method was used to measure the dosimetry reaction rate of several important threshold and non-threshold reactions, and

thermoluminescent dosimeters (TLDs) were used to measure the photon heating rate. Spectrum measurements were made during neutron generation by inserting counters into the experimental channels, repeatedly, changing detector position one after the other. Measurement of dosimetry reaction rates and gamma heating were made by inserting samples in the detector channels during neutron generation and irradiating at the same time for the required amount of time. The lithium glass scintillator was used to measure the tritium production rates (TPR). The experimental data and diagnostics are subject to errors which originate from the neutron yield, energy calibration, data processing (unfolding, fitting, normalization), different detectors, assemblies, and energy ranges, counting efficiency and statistics. The measurement errors are detailed in [12].

III.A. Computational Models and Methods

For the benchmark experiments, only the experimental assemblies are modeled. The experimental and target rooms, the geometry and materials of the detectors, the source angular distribution, the activation foils, the TLDs, and the fission chambers are not modeled in OpenMC. Rather we have simulated the neutron source as isotropic, even though the source energy and intensity are slightly dependent on the angle of emission with respect to the deuteron beam direction. Thus, the source spectrum of neutrons emitted toward the 0 degree direction was used in OpenMC and MCNP. According to the benchmark documentation, the D-T neutron source can be roughly described as an isotropic 14 MeV point source. The tungsten and beryllium assemblies are modeled in R-Z geometry with 31.45 cm equivalent radius, following the same approach in the MCNP input supplied with the SINBAD distribution. The experimental and target rooms, the geometry and materials of the detectors, the activation foils, the TLDs, and the fission chambers are not modeled in MCNP. However, the MCNP input features the source biasing variance reduction card to generate source neutrons emitted to the forward direction more than the backward direction with respect to the deuteron beam direction. Nuclear data from ENDF/B-VII.1 are employed to present the simulation results. The other major nuclear data libraries are tested on the neutron spectra of all the assemblies. Although these are not shown in the present report, since the neutron spectra differences observed from the different libraries are not large enough to be distinguished from each other in some cases and are planned to be presented in future work on nuclear data sensitivity analysis. The simulations are run with the number of histories to reduce the statistical error of tallied spectra to less than 5%. Whereas this

was not always the case for the secondary photon spectra in the high energy region where the statistical error can be more than 10% in some cases due to difficulty in convergence and much smaller number of secondary photons born at high energy. WW importance maps generated with DENOVO in the MAVRIC code system [13] are employed in the tungsten assembly calculations. Importance maps are not generated and not used in the vanadium and beryllium calculation due to the small size of the assemblies. Neutron only, and neutron-photon coupled simulations are performed and the radiation spectra, reaction rates, gamma heating, and TPR quantities are obtained using OpenMC cell tallies enclosing the detector locations in the experimental assemblies. The tallied flux in the unit of n-cm is converted to n/cm^2/lethargy by dividing by tally cell volume enclosing the detector location and lethargy of the energy groups, for comparison with measured spectra. The dosimetry reaction rates (^{27}Al $(n, \alpha)^{24}$Na, ^{93}Nb $(n, 2n)^{93m}$Nb, ^{115}In $(n, n')^{115m}$In, ^{58}Ni $(n, 2n)^{57}$Ni) and tritium production rate (^{6}Li $(n, t)^{4}$He) are calculated using the activation cross-sections from the International Reactor Dosimetry and Fusion File (IRDFF) library [14]. The other reaction rates are calculated using the transport cross-sections and then normalized to the atomic densities of the trace nuclides (^{197}Au, ^{235}U, ^{186}W) added to the materials to induce the reactions of interest. The gamma heating rate (GHR) is calculated to include contributions from electrons and positrons. OpenMC photon spectra are broadened with the energy-dependent window functions of the detector used in measurements. The csg2csg tool [15] was employed in translating the MCNP SINBAD inputs into XML geometry and materials input files for OpenMC. OpenMC Python API inputs are written for each benchmark experimental assembly described in the subsequent sections. The calculations in this paper are run with OpenMC version 0.14.1-dev.

In the sections that follow, OpenMC calculation results are compared to measured data from the FNS benchmark experiments and results from MCNP-6.2 and then discussed. MCNP-6.2 results are only shown for the flux spectra, TPR, and GHR, because they are important fusion neutronics parameters. The detector positions presented correspond to distances from the surface of the experimental assembly for the tungsten and vanadium, and distance from the target for the beryllium assembly. Comparisons to MCNP-6.2 results are commented upon in Section III.E.

III.B. FNS Clean Benchmark Experiment on Tungsten

The tungsten experimental assembly was made by stacking bricks of 50.7 m × 50.7 m square within thin aluminum support frames in quasi-cylindrical shape as shown in Fig. 1. The

purity of the tungsten is 94.8%, with nickel (2.1%) and copper (3.1%) impurities. The density of the tungsten is 18.05 g/cm^3. There were five detector positions on the assembly central axis: on the assembly front surface (0 mm), and inside at 76 mm, 228 mm, 380 mm, and 508 mm depths, for the measurement of the neutron and photon spectra, dosimetry reaction rates, and gamma heating.

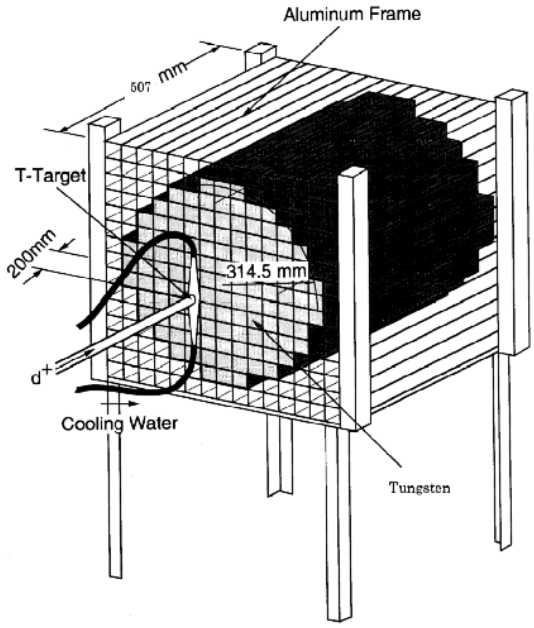

Fig. 1. Tungsten experimental assembly [12].

The calculated neutron spectra in the tungsten assembly are compared to the measured distribution for the detectors located at 76 mm, 228 mm, and 380 mm from the surface of the assembly in Fig. 2 (left). The PRC measurement in the keV region for the 76 mm detector location is up to 1440 keV. The measured neutron spectra at 228 mm and 380 mm measurement points have a wide peak in the 1 keV to 10 MeV region, and a broad dip in the 10 MeV region (also for the 76 mm detector location). Generally, the calculated neutron spectra follow the same trend as the measured one. The energy peak in the keV region by calculation slightly overestimates the measured data (PRC) at the 228 mm and 380 mm depths detector locations. Furthermore, the high energy (8 – 12 MeV) dip calculated overestimates the measured data at the 76 mm and 228 mm depths detector locations. This overestimation is confirmed by the slightly larger reaction rate of ^{93}Nb (n, $2n$)^{92m}Nb (threshold, 9 – 10 MeV) predicted by calculation in

comparison to measured data (see Table I). The high energy dip is well predicted at the 380 mm depth detector location.

For the photon flux spectra, the calculated results are also compared to the measured data in Fig. 2 (right) for detector positions 76 mm, 228 mm, and 380 mm. A large portion of the photons are produced at less than 7 MeV region. The calculated photon spectra agree with the measured data up to 4 MeV in the first detector position, 10 MeV in the second detector position, and throughout the photon energies in the third detector position. Beyond these energies, the photon flux underestimates the experiment, a discrepancy that could have been caused by large uncertainties of the (*n*, *gamma*) cross-section at high energy. The calculated photon spectra plotted in Fig. 2 has had its resolution broadened. Around 500 keV, sharp peak existed in the un-broadened tally estimates. The broadening has been performed to simulate the detector energy resolution by incorporating into the tally estimates the energy-dependent windows (resolution) of the detectors which are supplied with the experimental data in the SINBAD database.

The GHR calculated are compared to experimental data in Table II. Except for the measurement point closest to the source/target, the GHR are in good agreement with experiment. Moreover, the GHR calculated at all the measurement points are within the range of experimental uncertainty at one standard deviation. OpenMC underestimates the GHR measured at the point closest to the source/target. The experimental uncertainty at this point is large (58%).

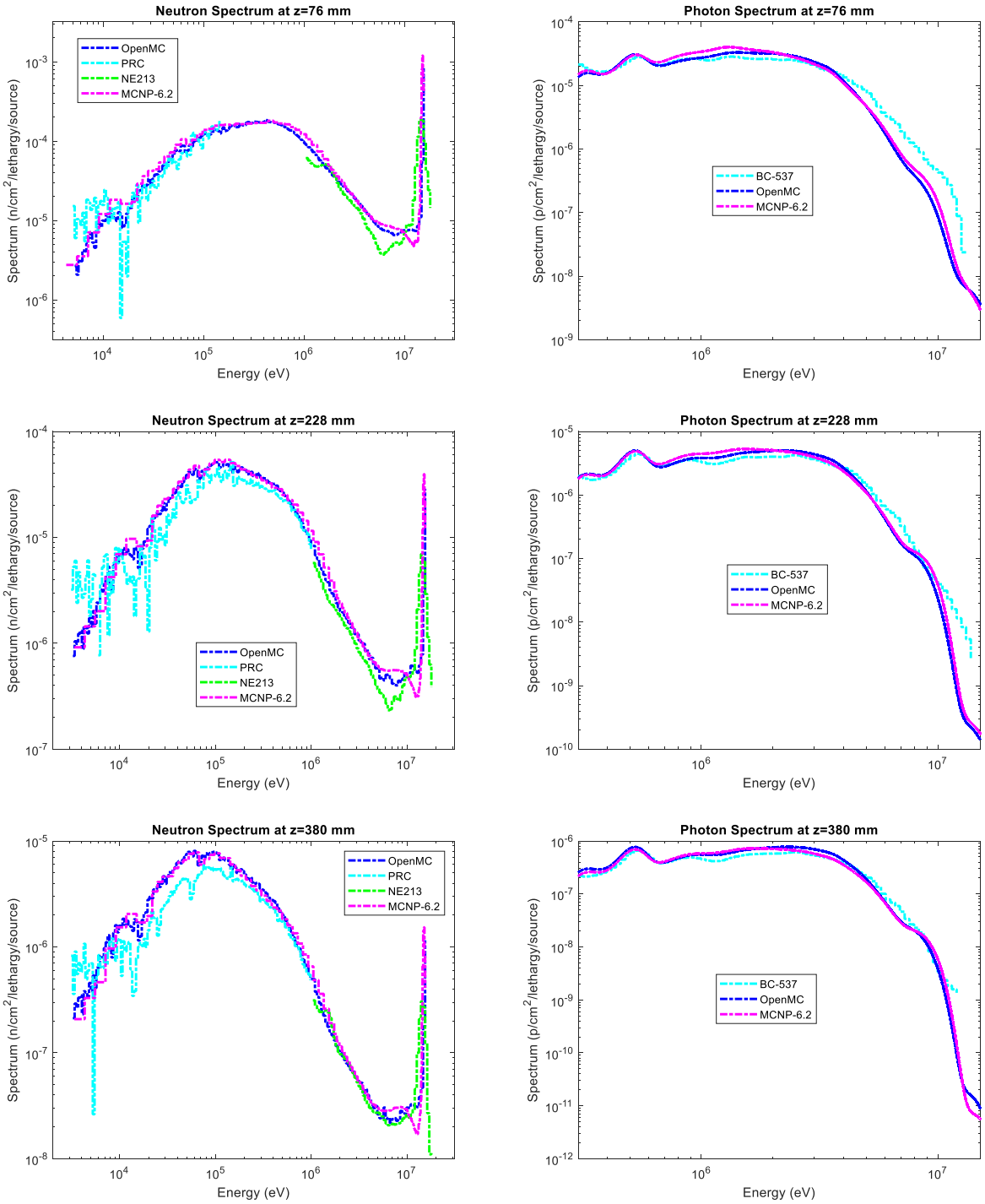

Fig. 2. Calculated and measured neutron flux and photon flux spectra, for detector positions at 76 mm, 228 mm, and 380 mm depths in the tungsten assembly.

Table I. Dosimetry reaction rates in tungsten assembly (reactions/atoms/source). Percent uncertainties in parentheses.

Detector position [mm]	^{27}Al (n, α)^{24}Na		
	Experiment	OpenMC	C/E
0	2.340E-29 (2.9)	2.262E-29 (0.0)	0.9665
76	4.270E-30 (3.1)	5.162E-30 (0.1)	1.2089
228	1.640E-31 (3.1)	2.021E-31 (0.3)	1.2323
380	6.600E-33 (4.7)	9.245E-33 (1.5)	1.4007
507	1.690E-33 (3.1)	4.668E-34 (6.9)	0.2762
Detector position [mm]	^{115}In (n, n')^{115m}In		
	Experiment	OpenMC	C/E
0	3.040E-29 (2.9)	2.747E-29 (0.1)	0.9036
76	1.470E-29 (3.0)	1.801E-29 (0.1)	1.2248
228	9.770E-31 (3.9)	1.170E-30 (0.2)	1.1980
380	4.710E-32 (7.2)	6.201E-32 (0.9)	1.3165
507	2.320E-32 (5.7)	2.515E-33 (4.5)	0.1084
Detector position [mm]	^{197}Au (n, γ)^{198}Au		
	Experiment	OpenMC	C/E
0	7.26E-29 (3.8)	3.859E-29 (0.1)	0.5316
76	1.51E-28 (4.7)	1.302E-28 (0.1)	0.8621
228	4.41E-29 (4.9)	5.145E-29 (0.1)	1.1667
380	8.23E-30 (7.7)	9.149E-30 (0.2)	1.1116
507	1.07E-29 (4.8)	3.227E-31 (0.8)	0.0302
Detector position [mm]	^{93}Nb (n, $2n$)^{92m}Nb		
	Experiment	OpenMC	C/E
0	1.010E-28 (2.9)	9.658E-29 (0.0)	0.9563
76	1.640E-29 (3.3)	2.126E-29 (0.1)	1.2962
228	6.000E-31 (3.2)	8.000E-31 (0.3)	1.3334
380	2.560E-32 (3.5)	3.566E-32 (1.6)	1.3930
507	4.720E-33 (3.2)	1.801E-33 (7.2)	0.3816
Detector position [mm]	^{186}W (n, γ)^{187}W		
	Experiment	OpenMC	C/E
0	2.270E-29 (3.1)	1.270E-29 (0.1)	0.5595
76	5.220E-29 (3.1)	3.922E-29 (0.0)	0.7514
228	1.580E-29 (3.0)	1.453E-29 (0.1)	0.9196
380	2.560E-30 (2.9)	2.474E-30 (0.2)	0.9666
507	1.690E-30 (2.9)	8.492E-32 (0.8)	0.0503

Table II. GHR in tungsten assembly (Gy/source). Percent uncertainties in parentheses.

Detector position [mm]	Experiment	OpenMC	C/E
0	5.41E-16 (58)	3.60E-16 (11.5)	0.6654
76	5.95E-16 (19)	5.95E-16 (0.1)	1.0004
228	9.38E-17 (17)	9.64E-17 (0.8)	1.0275
380	1.26E-17 (18)	1.45E-17 (1.6)	1.1512
Detector position [mm]	Experiment	MCNP-6.2	C/E
0	5.41E-16 (58)	3.76E-16 (0.3)	0.6951
76	5.95E-16 (19)	6.63E-16 (0.1)	1.1137
228	9.38E-17 (17)	1.02E-16 (0.1)	1.0848
380	1.26E-17 (18)	1.39E-17 (0.1)	1.1062

III.C. FNS Clean Benchmark Experiment on Vanadium

The vanadium assembly is shown in Fig. 3. It was a 254 mm side cube whose surfaces were covered by a 50.8 mm thick graphite reflector to minimize neutrons leaking out of the small assembly and background neutrons coming into the assembly from outside. The assembly is made up of vanadium cubic blocks whose sides are 50.8 mm. The vanadium is 99.777% pure with aluminum (0.073%), silicon (0.108%) and iron (0.042%) impurities. The assembly central axis houses three detector positions: on the assembly front surface (0 mm), and inside at 76.2 mm and 177.8 mm depth. The vanadium and graphite have densities of 6.033 g/cm^3 and 1.625 g/cm^3, respectively.

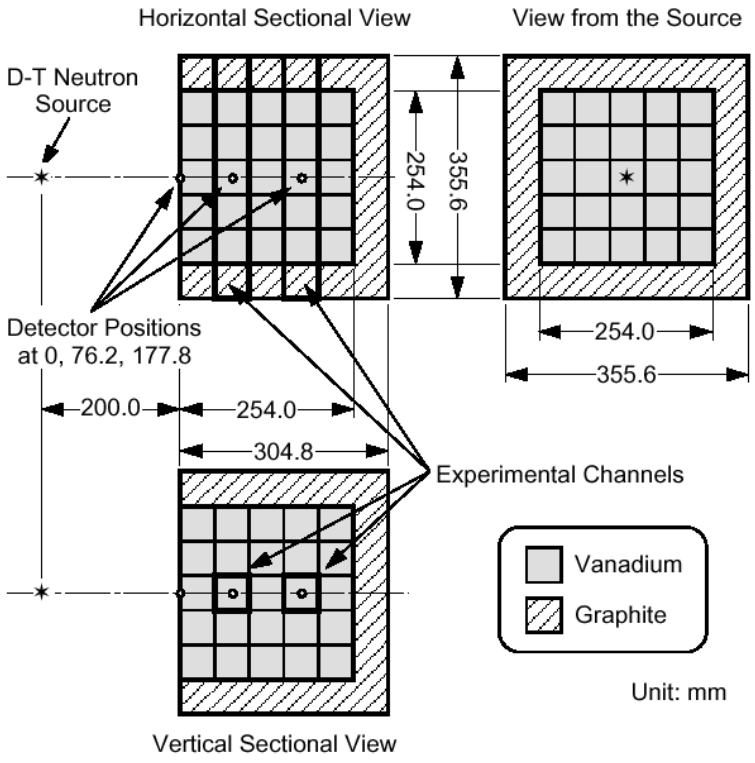

Fig. 3. Vanadium assembly surrounded by graphite reflector [16].

The calculated neutron spectra in the vanadium assembly are compared to the measured data for the detectors located at 76 mm and 178 mm from the surface of the assembly in Fig. 4 (top). The measured neutron spectra in the vanadium assembly are divided into three regions depending on the detector used. As seen in Fig. 4, the measured neutron spectra are well predicted by calculation from the keV to the MeV regions, including the high energy dip at 10 MeV. However, in the eV range, the calculated neutron spectra underestimate the measured data at all the detector locations. The low neutron flux in the eV region has been attributed to the small total cross section of vanadium [16]. In addition, this underestimation is consistent with the lower reaction rate of ^{197}Au $(n, \gamma)^{198}$Au compared to measured data (see Table III). Moreover, vanadium cross-sections have large uncertainties at high energy, although it is hard to relate this to the neutron flux discrepancy at low energy.

The photon flux spectra calculated are compared to the measured data in Fig. 5 (bottom) for detector positions at 76 mm and 178 mm. A large portion of the photons are produced in the energy range below 10 MeV. In this energy range, the calculated photon spectra agree with the measured data. The broadened peaks in the experimental spectrum are reproduced by broadening

the OpenMC spectra. Beyond 10 MeV, the photon flux underestimates the experiment. This is likely due to the large uncertainties of the (*n*, *gamma*) cross-section at high energy.

The GHR are shown in Table IV. At the detector positions 76 mm and 178 mm, the calculation slightly underestimates the experiment. The GHR at these positions are calculated within the experimental uncertainty at one standard deviation. At the 0 mm detector position, which is closest to the source/target and the surface of the vanadium assembly, the calculated GHR underestimates the experiment, although the calculation is within the experimental uncertainty at two standard deviations. The measured GHR at this position has a large uncertainty of 20%, so this could be a reason for the underestimation.

Table III. Dosimetry reaction rates in vanadium assembly (reactions/atoms/source). Percent uncertainties in parentheses.

Detector position [mm]	^{27}Al (n, α)^{24}Na		
	Experiment	OpenMC	C/E
0	2.320E-29 (3.33)	2.095E-29 (0.01)	0.9029
76	6.420E-30 (3.38)	5.708E-30 (0.03)	0.8890
178	1.340E-30 (3.26)	1.140E-30 (0.06)	0.8506
Detector position [mm]	^{115}In (n, n')^{115m}In		
	Experiment	OpenMC	C/E
0	3.400E-29 (3.26)	2.993E-29 (0.03)	0.8803
76	2.680E-29 (3.32)	2.501E-29 (0.03)	0.9334
178	9.160E-30 (3.42)	7.885E-30 (0.05)	0.8608
Detector position [mm]	^{197}Au (n, γ)^{198}Au		
	Experiment	OpenMC	C/E
0		2.863E-29 (1.21)	
76	1.62E-28 (3.25)	1.039E-28 (0.67)	0.6413
178	1.56E-28 (3.40)	1.018E-28 (0.93)	0.6523
Detector position [mm]	^{93}Nb (n, $2n$)^{92m}Nb		
	Experiment	OpenMC	C/E
0	1.000E-28 (3.51)	8.889E-29 (0.01)	0.8889
76	2.550E-29 (3.30)	2.310E-29 (0.03)	0.9060
178	5.270E-30 (3.53)	4.456E-30 (0.07)	0.8456

Table IV. GHR in vanadium assembly (Gy/source). Percent uncertainties in parentheses.

Detector position [mm]	Experiment	OpenMC	C/E
0	7.42E-16 (20.35)	7.11E-16 (3.73)	0.9582
76	7.25E-16 (9.31)	6.88E-16 (0.68)	0.9488
178	2.23E-16 (9.60)	2.23E-16 (1.25)	0.9243
Detector position [mm]	Experiment	MCNP-6.2	C/E
0	7.42E-16 (20.35)	6.59E-16 (0.50)	0.8879
76	7.25E-16 (9.31)	7.69E-16 (0.23)	1.0610
178	2.23E-16 (9.60)	2.28E-16 (0.28)	1.0205

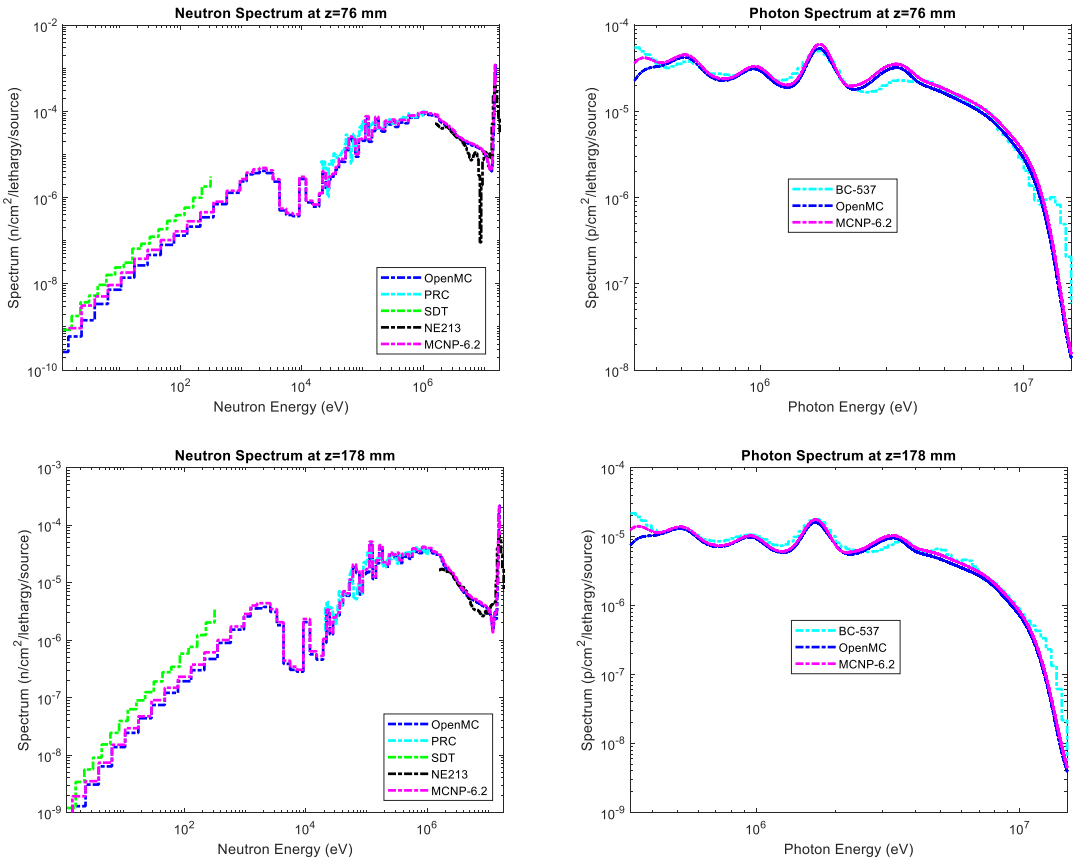

Fig. 4. Calculated and measured neutron flux and photon flux spectra, for detector positions at 76 mm and 178 mm, in the vanadium assembly.

III.D. FNS Clean Benchmark Experiment on Beryllium

The beryllium experimental assembly had the same quasi-cylindrical shape and stacked block dimensions as the tungsten assembly (Fig. 1). However, the beryllium assembly is 45.54 cm thick. There were eight detector positions on the assembly central axis where the neutron spectrum above 2 MeV was measured. In addition to reaction rates measurements, this experiment had the tritium production rate measured by the ^{6}Li (n, t)^{4}He reaction in a thin ^{6}Li-glass scintillator [17].

Fig. 5 illustrates the calculated neutron spectra in the beryllium assembly compared to measurements for the detectors located at 327 mm and 479 mm from the target. The PRC measurement in the keV region at 327 mm and 479 mm from the assembly surface is flat. In comparison to experiment, OpenMC predicts the neutron spectra reasonably well both in the keV and MeV regions. No photon spectra measurement was made in this experiment so no photon

spectra comparison could be carried out. The measured dosimetry reaction rates and TPR [18] are compared to calculations in Tables V, VI, and VII.

The fission reaction and tritium production rate obtained from calculations overestimates the measured data. It is difficult to conclude that this overestimation is caused by flux overestimation in the thermal energy region since the measured ^{197}Au $(n, \gamma)^{198}$Au reaction rate is not overestimated as can be seen in Table V. The overestimation is also reported in the documentations by the authors of this and other benchmarks using MCNP code and ENDF/B, JENDL, FENDL, and JEFF nuclear data libraries [17,19,20,21,22]. The overestimation of the tritium production rate has been attributed to parasitic absorption of thermal neutron induced by impurities present in the beryllium assembly. This is said to have reduced the measured tritium production rate. Besides, the effective thermal neutron absorption in the beryllium assembly is said to be 30% higher than the calculated one, according to the information given by the manufacturer. The overestimation was reduced in [21] by employing neutron thermal S(α,β) data for the transport in beryllium. In general, the calculated fission reaction and TPR by OpenMC follow the same trend as the measured one.

The ratio of calculated TPR/GHR to experimental TPR/GHR is summarized in Tables VIII and IX. Please note that the average *C*/*E* values shown in Tables VIII and IX, are not weighted with experimental uncertainties, they are the simple averages of the *C*/*E* values from each assembly in which the quantity of interest was measured. An average *C*/*E* ignores the "distance from D-T neutron source" dependence of the *C*/*E* values and places equal confidence level on all measurements (without outliers).

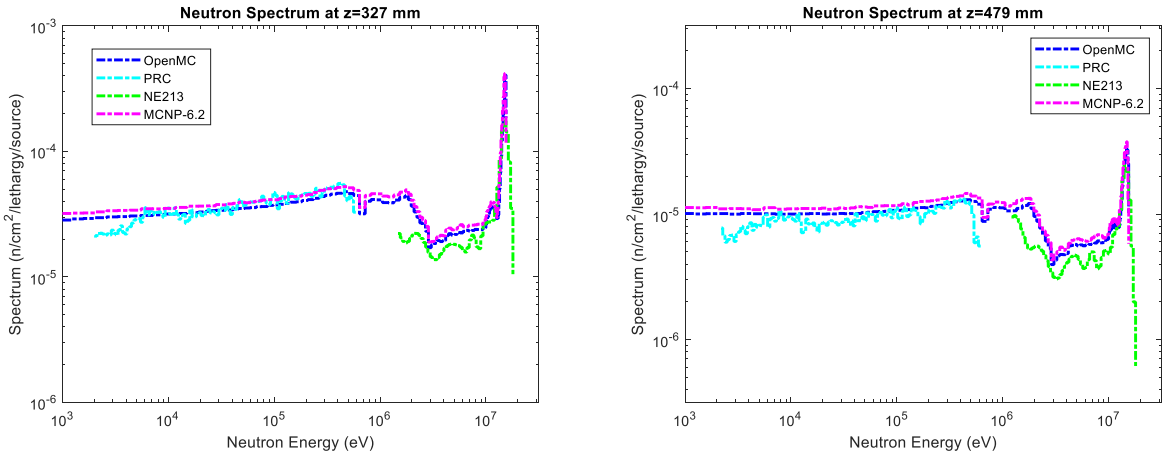

Fig. 5. Calculated and measured neutron flux spectra, for detector positions at 327 mm and 479 mm from the target, in the beryllium assembly.

Table V. Dosimetry reaction rates in beryllium assembly (reactions/atoms/source). Percent uncertainties in parentheses.

Detector position [mm]	^{27}Al (n, α)^{24}Na		
	Experiment	OpenMC	C/E
200	2.588E-29 (2.7)	2.012E-29 (0.0)	0.7776
349.2	3.750E-30 (3.0)	3.803E-30 (0.1)	1.0140
450.6	1.039E-30 (3.2)	8.290E-31 (0.2)	0.7979
552.0	2.853E-31 (3.7)	2.780E-31 (0.4)	0.9745
655.9	7.559E-32 (3.2)	9.284E-32 (0.7)	1.2282
Detector position [mm]	^{115}In (n, n')^{115m}In		
	Experiment	OpenMC	C/E
200	3.388E-29 (2.9)	3.142E-29 (0.1)	0.9275
349.2	1.719E-29 (2.9)	1.720E-29 (0.1)	1.0008
450.6	6.006E-30 (3.2)	5.027E-30 (0.1)	0.8370
552.0	1.925E-30 (3.4)	1.905E-30 (0.2)	0.9894
655.9	4.603E-31 (5.2)	6.027E-31 (0.4)	1.3094
Detector position [mm]	^{197}Au (n, γ)^{198}Au		
	Experiment	OpenMC	C/E
200	8.628E-27 (3.0)	1.260E-26 (0.4)	1.4601
349.2	7.272E-26 (3.0)	7.340E-26 (0.1)	1.0094
450.6	4.957E-26 (2.9)	4.674E-26 (0.1)	0.9429
552.0	2.330E-26 (2.9)	2.342E-26 (0.1)	1.0052
655.9	2.151E-27 (3.0)	4.492E-27 (0.3)	2.0884
Detector position [mm]	^{93}Nb (n, $2n$)^{92m}Nb		
	Experiment	OpenMC	C/E
200	9.933E-29 (2.7)	8.238E-29 (0.0)	0.8294
349.2	1.305E-29 (2.9)	1.292E-29 (0.1)	0.9902
450.6	3.326E-30 (3.1)	2.570E-30 (0.2)	0.7728
552.0	9.015E-31 (3.1)	8.197E-31 (0.3)	0.9093
655.9	2.295E-31 (3.3)	2.676E-31 (0.6)	1.1659
Detector position [mm]	^{58}Ni (n, $2n$)^{57}Ni		
	Experiment	OpenMC	C/E
200	9.416E-30 (2.9)	7.258E-30 (0.0)	0.7709
349.2	6.881E-31 (3.6)	7.509E-31 (0.1)	1.0913
450.6	1.338E-31 (4.3)	1.111E-31 (0.2)	0.8306
552.0	3.271E-32 (4.5)	2.930E-32 (0.4)	0.8956
655.9	7.543E-33 (9.0)	8.080E-33 (0.8)	1.0712

Table VI. Fission reaction rates in beryllium assembly (fission/atom/source). Percent uncertainties in parentheses.

Detector position [mm]	Experiment	OpenMC	C/E
241.2	9.267E-26 (3.81)	1.169E-25 (0.06)	1.2612
266.6	1.307E-25 (3.80)	1.434E-25 (0.05)	1.0972
292.0	1.579E-25 (3.80)	1.971E-25 (0.04)	1.2485
317.4	1.794E-25 (3.80)	2.138E-25 (0.04)	1.1918
342.8	1.906E-25 (3.80)	2.237E-25 (0.04)	1.1739
419.0	1.771E-25 (3.80)	2.091E-25 (0.04)	1.1810
469.8	1.432E-25 (3.80)	1.768E-25 (0.04)	1.2348
520.6	1.073E-25 (3.80)	1.243E-25 (0.05)	1.1584
571.4	7.071E-26 (3.80)	6.995E-26 (0.06)	0.9893
622.2	3.368E-26 (3.81)	4.347E-26 (0.08)	1.2907

Table VII. TPR in beryllium assembly (tritium/atom/source). Percent uncertainties in parentheses.

Detector position [mm]	Experiment	OpenMC	C/E
201.1	3.583E-26 (3.07)	2.910E-26 (0.12)	0.8122
251.7	2.065E-25 (3.19)	2.353E-25 (0.05)	1.1396
302.3	2.983E-25 (3.06)	3.243E-25 (0.04)	1.0872
327.6	3.226E-25 (2.35)	3.521E-25 (0.04)	1.0913
403.5	3.254E-25 (2.35)	3.617E-25 (0.04)	1.1117
479.4	2.339E-25 (2.92)	2.915E-25 (0.04)	1.2464
504.7	2.007E-25 (2.92)	2.493E-25 (0.04)	1.2422
605.9	7.863E-26 (2.71)	7.163E-26 (0.08)	0.9109
631.2	5.050E-26 (3.01)	3.150E-26 (0.10)	0.6237
Detector position [mm]	Experiment	MCNP-6.2	C/E
201.1	3.583E-26 (3.07)	3.253E-26 (1.78)	0.9078
251.7	2.065E-25 (3.19)	2.635E-25 (0.70)	1.2760
302.3	2.983E-25 (3.06)	3.643E-25 (0.61)	1.2211
327.6	3.226E-25 (2.35)	3.952E-25 (0.58)	1.2251
403.5	3.254E-25 (2.35)	4.075E-25 (0.58)	1.2523
479.4	2.339E-25 (2.92)	3.253E-25 (0.59)	1.3908
504.7	2.007E-25 (2.92)	2.791E-25 (0.64)	1.3904
605.9	7.863E-26 (2.71)	8.026E-26 (1.09)	1.0207
631.2	5.050E-26 (3.01)	3.531E-26 (1.49)	0.6992

Table VIII. TPR calculation-experiment comparison result.

Assembly	Number of measurements		OpenMC	
			Mean	Std. dev
Beryllium	9	*C/E*	1.0295	0.1956

Table IX. GHR calculation-experiment comparison result.

Assembly	Number of measurements		OpenMC	
			Mean	Std. dev
Vanadium	3	*C/E*	0.9437	0.0143
Tungsten	4	*C/E*	0.9611	0.1799
Overall	7	*C/E*	0.9537	0.1366

III.E. Comparison to MCNP-6.2

In Fig. 2, 4, and 5, MCNP-6.2 simulation results of the benchmark problems are included in the plots. Please note that MCNP-6.2 results are based on ENDF-B/VII.1 nuclear data. In addition, the MCNP-6.2 inputs from SINBAD include cell based WW importance and source biasing VR cards. In Fig. 2, 4, and 5, OpenMC and MCNP-6.2 neutron spectra results agree well, following the same trend. However, in Fig. 2, slight discrepancy at high energy is noticed in the tungsten assembly neutron spectra between OpenMC and MCNP-6.2. Furthermore, both codes overestimate the PRC detector data between 20 keV to 1 MeV at the 228 mm and 380 mm locations in the tungsten assembly (See Fig. 2). The two codes underestimate the neutron spectra in the vanadium assembly at low neutron energy (See Fig. 4), implying that the underestimation could be a nuclear data issue. In the beryllium assembly, MCNP-6.2 predicts a 12% higher neutron flux (on average) than OpenMC (See Fig. 5). The photon spectra from the two codes are in good agreement, showing peaks at identical energies. These photon peaks are broadened as described in Section III.A. In Table VII, MCNP-6.2 overestimates the measured tritium production rate and those calculated by OpenMC in the beryllium assembly. Moreover, in Tables II and IV, MCNP-6.2 predicts a 9% greater GHR (on average), compared to OpenMC, in the tungsten and vanadium assemblies, at five detector locations out of seven. In general, the OpenMC versus MCNP-6.2 verification indicates comparable accuracy of the flux spectra, gamma heating and TPR.

IV. Conclusions and perspectives

This work adds to the growing validation of OpenMC's fusion neutronic capabilities by analyzing fusion neutronics shielding clean benchmark experiments conducted at the JAERI's FNS facility. The neutron and photon spectra, reaction rates, gamma heating and TPR are calculated by OpenMC and compared to experimental data and results from MCNP-6.2. The comparison indicates comparable accuracy and that OpenMC can be used to analyze the benchmark experiments. The average calculated-to-experimental ratio in the beryllium assembly is 1.03 ± 0.20 for the TPR and 0.95 ± 0.14 for the GHR in the vanadium and tungsten assemblies. The observed discrepancies are likely due to three sources: uncertainties in nuclear data, measurement uncertainties, and modeling parameter uncertainties. For instance, the nuclear data of vanadium in low neutron energy region needs to be improved. A number of comments on the previously mentioned uncertainties could be given. For example, the GHR measured in tungsten and vanadium have large uncertainties at detector locations closest to the source. There is the source angular distribution, which is not modeled. Besides, tungsten and vanadium have large (*n*, *gamma*) cross-section uncertainties at high energy. The threshold reactions dominate the locations closest to the source and non-threshold reactions such as radiative capture dominate locations far from the source. The large uncertainties of nuclear data at high energies could be one of the reasons for the discrepancies observed close to the source.

MCNP realistic modeling of the tungsten and vanadium assemblies reported in [23] to include the experimental and target rooms, the D-T source angular distribution, and the use of dosimetry cross section for reaction rates in the activation foils shows that the results from realistic model do not differ significantly from those of the simplified model which considers only the experimental assemblies, when compared to experiments. This is particularly true for neutron and photon spectra. However, the modeling uncertainties are likely to be responsible for the discrepancies observed in the reaction rates, such as lack of modeling the actual detector geometry, materials, activation foils, self-shielding effects, and back scattering from the experimental room. The report [23] provides a sensitivity of calculated nuclear responses to the fidelity of the modeling in the tungsten and vanadium experimental assemblies.

This study is based on the computation models of the benchmarks in which the source angular distribution, experimental/target room (and back scattered particles), actual geometries of the detectors, activation foils, streaming, and self-shielding effects, are not modeled. Although the computational models are simplified, the results obtained show that it represents a good first

preliminary validation effort using approximate modeling and future efforts are needed to develop more representative and realistic computational models.

Additional steps to extend the range of fusion neutronics shielding problems to be analyzed are underway. Future work will focus on nuclear data uncertainty quantification and sensitivity analysis in OpenMC fusion neutronic calculations. Nuclear data uncertainties will be propagated to quantify the TPR, gamma heating and shut down dose rates uncertainties. Sensitivities of fusion neutronics responses to the cross-section data will be analyzed. Moreover, further V&V of OpenMC VR, radiation shielding and deep penetration capabilities, including figure of merit comparisons for analog and non-analog simulations will be performed. The Python API inputs and automated output processing tool for these benchmarks will be made publicly available.

References

1. Valentine, T. Berry, S. Bradnam, J. Hagues, J. Hodson, Benchmarking of emergent radiation transport for fusion neutronics applications, Fusion Eng. Des., 180 (2022) 113197. https://doi.org/10.1016/j.fusengdes.2022.113197
2. J. W. Bae, E. Peterson, J. Shimwell, AR reactor neutronics multicode validation, Nucl. Fusion 62 (2022) 066016. https://doi.org/10.1088/1741-4326/ac5450.
3. T. Eade, B. Colling, J. Naish, et al., Shutdown dose rate benchmarking using modern particle transport codes, Nucl. Fusion 60 (2020) 056024. https://doi.org/10.1088/1741-4326/ab8181.
4. X. Zhang, P. Shriwise, S. Liu, Implementation and verification of PyNE R2S with DAG-OpenMC, Fusion Eng. Des., 160 (2020) 111837. https://doi.org/10.1016/j.fusengdes.2020.111837.
5. Y. Hu, Y. Qiu, U. Fischer, Development and benchmarking of the weight window mesh function for OpenMC, Fusion Eng. Des., 170 (2021) 112551. https://doi.org/10.1016/j.fusengdes.2021.112551
6. Y. Hu, S. Yan, Y. Qiu, Implementation and benchmarking of the local weight window generation function for OpenMC, Nucl. Eng. Tech., 54 (2022) 3803 – 3810, https://doi.org/10.1016/j.net.2022.04.021.

7. P. K. Romano, N. E. Horelik, B. R. Herman, et al., OpenMC: a state-of-the-art Monte Carlo code for research and development, Ann. Nucl. Energy 82 (2015) 90 – 97. https://doi.org/10.1016/j.anucene.2014.07.048
8. I. A. Kodeli, E. Sartori, SINBAD – radiation shielding benchmark experiments, Ann. Nucl. Energy 159 (2021) 108254, https://doi.org/10.1016/j.anucene.2021.108254.
9. I. Kodeli, G. Zerovnik, A. Milocco, Examples of use of SINBAD database for nuclear data and code validation, EPJ Web Conf., 153 (2017), https://doi.org/10.1051/epjconf/201715302010, 02010.
10. J. Yu, B. Forget. Verification of depletion capability of OpenMC using VERA depletion bencnhmark. Ann. Nucl. Energy 170 (2022) 108973. https://doi.org/10.1016/j.anucene.2022.108973
11. openmc; https://github.com/openmc-dev/openmc.git (current as of Nov. 27, 2023).
12. F. Maekawa, C. Konno, Y. Kasugai, et al., Data collection of fusion neutronics benchmark experiment conducted at FNS/JAERI. JAERI-Data/Code 98-021, Japan Atomic Energy Research Institute, 1998.
13. D. E. Peplow, Monte Carlo Shielding Analysis Capabilities with MAVRIC, Nucl. Tech., 174, 2, 289 (2011); https://doi.org/10.13182/NT174-289.
14. A. Trkov, P.J. Griffin, S.P. Simakov et al., IRDFF-II: A new neutron metrology library. Nucl Data Sheets, 163 (2020) 1 – 108. https://doi.org/10.1016/j.nds.2019.12.001
15. A. Davis, S. Lilley, J. Shimwell, csg2csg: a tool to assist validation & verification, in European Physical Journal Web of Conferences, 247, 04012 (2021). https://doi.org/10.1051/epjconf/202124704012.
16. F. Maekawa, Y. Kasugai, C. Konno, et al., Benchmark experiment on vanadium with D-T neutrons and validation of evaluated nuclear data libraries by analysis of the experiment, J. Nucl. Sci. Tech., 36 (3), 242-249 (1999). https://doi.org/10.1080/18811248.1999.9726204
17. Collection of experimental data for fusion neutronics benchmark, (Ed.) Sub Working Group of Fusion Reactor Physics Subcommittee, JAERI-M 94-014, Japan Atomic Energy Research Institute, 1994.
18. H. Maekawa, S. Yamaguchi, C. Konno, et al., Benchmark experiment and analysis of a beryllium cylindrical assembly, Fusion Tech., 19 (3P2B) 1949 – 1954, 1991. https://doi.org/10.13182/FST91-A29627

19. F. Maekawa, M. Wada, C. Ichihara, et al., Compilation of Benchmark Results for Fusion Related Nuclear Data. JAERI-Data/Code 98-024, Japan Atomic Energy Research Institute, 1998.
20. Y. M. Verzilov, K. Ochiai, S. Sato, et al., Analysis of impurities in beryllium, affecting evaluation of the tritium breeding ratio. JAERI-Research 2004-005, Japan Atomic Energy Research Institute, 2004.
21. Y. Verzilov, S. Sato, K. Ochai, et al., The integral experiment on beryllium with D-T neutrons for verification of tritium breeding, Fus. Eng. Des., 82 (2007) 1 – 9. https://doi.org/10.1016/j.fusengdes.2005.12.007
22. K. Kondo, K. Ochiai, Y. Tatebe, et al., Integral experiment on beryllium with DD neutrons for nuclear data benchmarking, Prog. Nucl. Sci. Tech., 1 (2011) 61 – 64. https://doi.org/10.15669/pnst.1.61
23. A. Milocco, The quality assessment of the FNS benchmark experiments, IJS Internal Report, IJS-DP-10215, Institut Jožef Stefan, 2009.